2021 43rd Annual International Conference of the
IEEE Engineering in Medicine & Biology Society (EMBC)
Oct 31 - Nov 4, 2021. Virtual Conference

Deep Learning for Predicting Gamma-Ray Interaction Positions in LYSO Detector

C. Clement[1], G. Birindelli[1], M. Pizzichemi[2], F. Pagano[2], M. Kruithof-de Julio[3], A. Rominger[1], E. Auffray[2], K. Shi[1]

Abstract— **Positron Emission Tomography (PET) is among the most commonly used medical imaging modalities in clinical practice, especially for oncological applications. In contrast to conventional imaging modalities like X-ray Computed Tomography (CT) or Magnetic Resonance Imaging (MRI), PET retrieves in vivo information about biochemical processes rather than just anatomical structures. However, physical limitations and detector constraints lead to an order of magnitude lower spatial resolution in PET images. In recent years, the use of monolithic detector crystals has been investigated to overcome some of the factors limiting spatial resolution. The key to increasing PET systems' resolution is to estimate the gamma-ray interaction position in the detector as precisely as possible.**

In this work, we evaluate a Convolutional Neural Network (CNN) based reconstruction algorithm that predicts the gamma-ray interaction position using light patterns recorded with Silicon photomultipliers (SiPMs) on the crystal's surfaces. The algorithm is trained on data from a Monte Carlo Simulation (MCS) that models a gamma point source and a detector consisting of Lutetium–yttrium oxyorthosilicate (LYSO) crystals and SiPMs added to five surfaces. The final Mean Absolute Error (MAE) on the test dataset is 1.48 mm.

I. INTRODUCTION

Since its introduction in a clinical context in the 1970s, PET performance has increased ten times in spatial resolution and forty times in sensitivity [1]. Today, PET is one of the most widely used medical imaging modalities due to its ability to measure metabolic activity in a patient's body.

However, PET systems' spatial resolution is limited compared to other medical imaging modalities like CT and MRI. It is constrained by several degrading factors, such as the distance that a positron travels before annihilating with an electron, scattering of the emerging gamma-rays in the tissue, and the detector's resolution.

There has been a trend in pre-clinical PET research towards using monolithic detector crystals instead of pixelated ones to increase the spatial resolution in recent years. The advantage of monolithic crystals is that the resolution is not inherently limited by the pixel size but can be improved with more advanced readout schemes and data processing methods.

Wang et al. [2] developed a monolithic PET detector system that can estimate gamma-ray interaction positions with Neural Networks (NNs). One network was trained to estimate the plane position and another to predict the Depth of Interaction (DOI). The input data were created with a simplified readout scheme with signals from a Photomultiplier Tube (PMT) on one side of the crystal.

Marcinkowski et al. [3] investigated a high-resolution small-animal PET system based on a continuous crystal. In this system, a LYSO crystal is coupled with a Digital Photon Counter, and the gamma-ray interaction position is determined using mean nearest neighbor positioning.

Tao et al. [4] compare four different neural network architectures that estimate gamma-ray interaction positions in monolithic crystals. Fully connected and convolutional networks with regression and classification heads are trained with mean detector response functions as input. The authors note that deep learning methods reduce the memory cost by a factor of one to two orders of magnitude compared to searching-based methods.

The work by Sanaat and Zaidi [5] presents another approach to estimate the DOI in a monolithic crystal using a NN. They trained a multilayer perceptron with data from a MCS that outputs the 3D gamma-ray interaction position. Notably, the proposed approach improves the spatial resolution of the PET system compared to analytical methods.

In this work, we want to predict the gamma-ray interaction position inside a monolithic crystal as precisely as possible using the light patterns recorded with SiPMs on the crystal's surfaces that emerge through scintillation. For the prediction, a CNN based approach is used that takes the surface light patterns as input and outputs the interaction point. We create a dataset consisting of hundreds of thousands of light patterns and corresponding interaction points with a MCS to train the CNN. In the simulation, we model a detector made up of LYSO crystals with SiPMs added to all surfaces except for the front one.

II. METHODS

A. Geant4 Simulation of Gamma Point Source and LYSO Detector

The MCS containing a gamma point source and a LYSO detector is built with the Geant4 simulation toolkit [6], [7], [8]. With Geant4, "the passage of particles through matter" can be simulated for a wide range of physics processes, particles, and materials over a broad energy spectrum. A Geant4 application program consists of several parts covering all aspects of a simulation: detector construction, primary particle generation, physics processes, detector response, data generation, and visualization.

This work was supported by the Swiss National Science Foundation under grant SNFN 200021_188914.

[1]Inselspital, Department of Nuclear Medicine, Bern, Switzerland
[2]CERN, EP department, Geneva, Switzerland
[3]Inselspital, Department of Biomedical Research , Bern, Switzerland

1) Detector Construction: The detector is a 60 x 120 x 20 mm^3 box-shaped volume consisting of three box-shaped LYSO crystals with a volume of 60 x 40 x 20 mm^3 each. The crystals' optical surfaces are created with Geant4's `unified` model and `ground` finish with a sigma alpha value of 0.01 and a specular lobe constant of 1.0. The three crystals are optically decoupled from each other through a 0.1 mm thick air gap between them. The crystal-air optical border surfaces are created with Geant4's `unified` model and `polishedbackpainted` finish.

To all surfaces except the front one, where the gamma-rays enter the crystal, SiPMs are added. To simulate the optical coupling between crystals and SiPMs, a 0.10 mm thick layer of optical grease and 0.31 mm thick glass plates are inserted before a 1.0 mm thick silicon layer. The complete detector system is placed in a surrounding volume made up of `G4_Galactic` material. Fig. 1 shows a schematic of the setup, and the optical properties of the simulated materials are given in Table I.

TABLE I

OPTICAL PROPERTIES OF THE MATERIALS IN THE SIMULATION. ENTRIES WITH AN ASTERISK ARE DEPENDENT ON PHOTON ENERGY. THE VALUES FOR THE SCINTILLATION YIELD OF SILICON ARE TAKEN FROM [9] AS FOUND IN [10].

	LYSO	Opt. Grease	Glass	Si
Density [g/cm^3]	7.1	1.06	2.40	2.33
Refr. Index	*	1.46	1.51	*
Scint. Yield [Photons/MeV]	40,000			
Fast Time Const. [ns]	36			
Resolution Scale	4.8			
Fast Scint. Rise Time [ps]	50			
Abs. Length [m]	*			

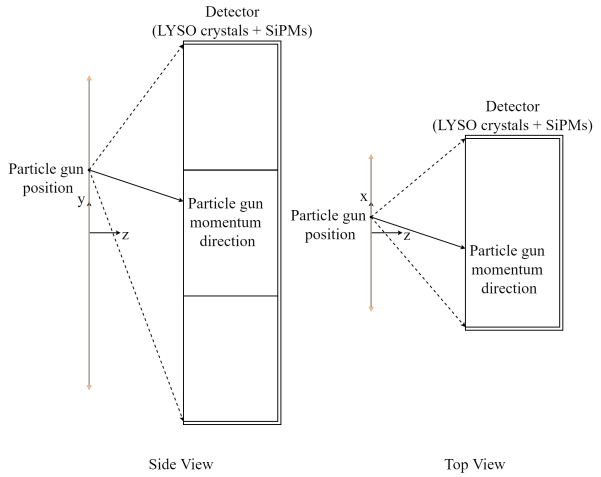

Fig. 1. Schematic of the detector setup viewed from the side and top. The detector is made up of three LYSO crystals with SiPMs added to all surfaces except for the front one. The position of the point source is chosen randomly from the orange plane and the momentum direction is selected randomly under the condition that the crystal is hit.

2) Primary Particle Generation: In the simulation, a particle gun emits primary gamma particles with an energy of 511 keV. To create a dataset with a large variety of gamma-ray interaction positions in the crystal, the particle gun's position and momentum direction are randomized. The position is randomly chosen from a surface parallel to the detector's front surface that has a distance of 30 mm to it. The momentum direction is then randomly selected under the condition that the crystal is always hit. The randomized position and momentum direction are illustrated in Fig. 1.

3) Analysis: Geant4's analysis manager is set up to save the desired outputs of the simulation. In this work, these are the interaction positions of the gamma-ray in the crystal and the positions of the optical photons entering the silicon layer.

B. SiPM Simulation

The SiPM array simulated in this work is Hamamatsu's S13615-1050N-16 [11], whose properties are described in Table II.

Except for the front surface, all of the detector's surfaces are entirely covered with SiPM arrays. They are simulated with the following procedure that accounts for the dead space between each SiPM array and between each single SiPM:

1) Create 2D histograms of optical photons entering the silicon layer for each crystal surface covered with SiPMs.
2) Split each histogram in 20 x 20 mm^2 blocks.
3) Remove the border of each block such that its dimensions equal the dimensions of the SiPM array.
4) Split the SiPM array block into 16 x 16 SiPM blocks.
5) Remove the border of each SiPM block to account for the dead space between each SiPM.
6) Compute the output value of each SiPM by counting the number of photons going through it and multiplying that number by the photon detection efficiency of the SiPM.

TABLE II

PROPERTIES OF THE SIMULATED SIPM ARRAY [11].

Channels	16 x 16
Photosensitive Area per Channel [mm^2]	1.0 x 1.0
Dimensions [mm^2]	19.25 x 19.25
Pixel Pitch [µm]	50
Pixels per Channel	396
Fill Factor [%]	74
Max. Photon Detection Efficiency [% at 450 nm]	40

C. Dataset Creation

The Geant4 simulation described in subsection II-A is run in parallel to create the train and test datasets. Each simulation runs one event, i.e. one primary gamma particle, and creates one output file containing the gamma-ray interaction positions and one containing the positions of the optical photons entering the silicon layer. These output files are then further processed to create the light patterns as described in subsection II-B. Additionally, the light patterns are padded such that they all have the same square shape. A training dataset of 140,000 samples and a test dataset of 14,000

samples are created in this manner. An example sample is shown in Fig. 2.

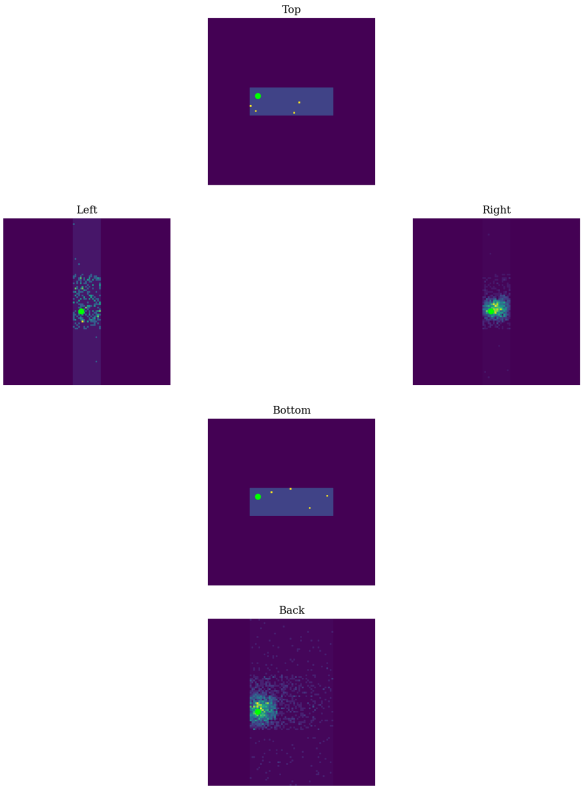

Fig. 2. Example sample showing the light patterns recorded with the SiPMs on all surfaces of the detector except the front one. The light patterns created through the SiPM simulation are padded such that they all have the same square shape. The green dot is the interaction position of the gamma-ray inside the crystal projected onto each surface. As the interaction occured in the middle crystal, almost no photons are recorded on the top and bottom surfaces.

D. Interaction Position Prediction

The created dataset is used to train a CNN based reconstruction network that predicts the gamma-ray interaction position inside the crystal. The input to the network is the light patterns recorded with SiPMs on the detector's surface. With these light pattern images, the network learns the non-linear relationship between the images and the gamma-ray interaction position.

1) Baseline Method: In addition to our deep learning based approach, a simple centroiding based method is implemented to serve as a baseline.

For every sample in the dataset, the following steps are performed to determine the interaction position:

1) Compute the centroids of every light pattern.
2) Take the mean of the centroids of corresponding light patterns (top-bottom, left-right) to compute XZ- and YZ-centroids (not applicable for the back light pattern as there is no corresponding front light pattern).
3) Take the mean of the corresponding dimensions of the XY-, XZ-, and YZ-centroids to compute the X-, Y-, and Z-centroid.
4) Stack the X-, Y-, and Z-centroid to create the predicted XYZ-position.

The predicted position is then compared to the ground truth value for every sample in the dataset.

2) Training Pipeline: PyTorch Lightning [12] is used to implement the training pipeline. The code is organized with subclasses of the `LightningDataModule` and the `LightningModule`. With the `LightningDataModule` subclass, the train and test datasets are loaded, the train dataset is split into a train and a validation dataset, and the PyTorch `DataLoaders` are set up. With the `LightningModule` subclass, the network architecture, loss function, and optimizer are initialized. Additionally, the training, validation, and test steps are defined, including the logging of the loss. Weights & Biases [13] is used to create experiment sweeps and log results.

3) Experiment Setup: In this work, the trade-off between the number of surfaces covered with SiPMs and interaction point prediction performance is investigated. The parameters given in Table III are used for every experiment run. The experiments are performed on a machine with a NVIDIA GeForce RTX 2080 Ti GPU. One run takes approximately 10 minutes.

TABLE III
PARAMETERS USED FOR EVERY EXPERIMENT RUN. THE NUMBER OF INPUT CHANNELS C IS DETERMINED BY THE NUMBER OF SURFACES WITH SIPMS.

Dataset Splits	110k train, 30k val, 14k test
Input Tensor Size	Cx96x96
Network Architecture	ResNet18 [14]
Loss Function	Mean Absolute Error (MAE)
Optimizer	Adam [15]
Learning Rate	3e-4
Batch Size	256
Epochs	20

III. RESULTS & DISCUSSION

A. Baseline

The centroiding based baseline algorithm described in subsubsection II-D.1 reaches a MAE of 6.16 mm on the test dataset.

This value serves as a baseline for the following experiment that uses a deep learning based approach.

B. Number of Surfaces Covered in SiPMs

With this experiment, the trade-off between prediction performance and the number of detector surfaces covered with SiPMs used as input for the network is evaluated. The runs are all performed using the parameters from Table III with varying input channels corresponding to the choice of surfaces used for the run. In total, there are 31 runs in this experiment, as every possible combination of the five surfaces is used. The test results of the runs are shown in Table IV.

These results show that some surfaces encode significantly more information compared to others. The back surface has

the greatest predictive influence, improving performance by 470.76 % compared to the least predictive surface, the bottom one. Besides, the back surface is also part of every other best performing combination of light patterns.

Notably, the best result with a test MAE of 1.48 mm is not achieved using all five possible surfaces but with only the following three surfaces: back, left, and right. Adding the bottom and top surface leads to worse performance as those two surfaces seem to encode no additional information about the interaction position. The optical decoupling of the crystals can explain this performance decrease. If the gamma-ray interaction occurs in the middle crystal, almost no photons exit the top and bottom surfaces and thus, the top and bottom light pattern images do not contain any valuable information. If the interaction occurs in the top or bottom crystal, then either the bottom or top light pattern encodes no useful information.

TABLE IV

TEST RESULTS OF THE NUMBER OF INPUT-LIGHT-PATTERNS EXPERIMENT. THE BEST PERFORMING COMBINATION FOR EVERY NUMBER OF LIGHT PATTERNS IS SHOWN IN BOLD. THE RELATIVE IMPROVEMENT IS COMPUTED BASED ON THE WORST RESULT. THE FIRST TWO LETTERS OF EACH SURFACE NAME ARE USED TO ABBREVIATE THE SURFACES: BA - BACK, TO - TOP, BO - BOTTOM, LE - LEFT, RI - RIGHT.

	Surfaces	Test MAE [mm]	Rel. Improv. [%]
1	**ba-le-ri**	1.48	529.62
2	**ba-to-bo-le-ri**	1.52	526.79
3	**ba-to-le-ri**	1.55	525.30
4	ba-bo-le-ri	1.56	524.43
...			
8	ba-to-ri	1.78	509.73
9	**ba-le**	1.80	508.36
10	ba-to-bo-ri	1.80	508.23
...			
19	ba-to	2.25	477.88
20	**ba**	2.35	470.76
21	to-bo-ri	2.85	437.40
...			
31	bo	9.33	0.00

IV. CONCLUSIONS

In this work, the gamma-ray interaction position in a monolithic detector system is reconstructed with a CNN using the light patterns that emerge on the detector's surface. Our experiments showed that some light patterns encode significantly more information for the network compared to others. Further experiments will be performed by evaluating a varying number of crystals per side and different optical (de-)coupling methods. These results will directly influence the design of the prototype system consisting of two of the described detectors.

REFERENCES

[1] T. Jones and D. W. Townsend, "History and future technical innovation in positron emission tomography," *Journal of Medical Imaging*, vol. 4, p. 011013, Mar. 2017.

[2] Y. Wang, W. Zhu, X. Cheng, and D. Li, "3D position estimation using an artificial neural network for a continuous scintillator PET detector," *Physics in Medicine and Biology*, vol. 58, pp. 1375–1390, Feb. 2013.

[3] R. Marcinkowski, P. Mollet, R. V. Holen, and S. Vandenberghe, "Sub-millimetre DOI detector based on monolithic LYSO and digital SiPM for a dedicated small-animal PET system," *Physics in Medicine and Biology*, vol. 61, pp. 2196–2212, Feb. 2016.

[4] L. Tao, X. Li, L. R. Furenlid, and C. S. Levin, "Deep Learning Techniques for Gamma Ray Interaction Location Estimation in Monolithic Scintillation Crystal Detectors," in *2018 IEEE Nuclear Science Symposium and Medical Imaging Conference Proceedings (NSS/MIC)*, pp. 1–3, Nov. 2018.

[5] A. Sanaat and H. Zaidi, "Accurate estimation of depth of interaction in PET on monolithic crystal coupled to SiPMs using a deep neural network and Monte Carlo simulations," in *2019 IEEE Nuclear Science Symposium and Medical Imaging Conference (NSS/MIC)*, pp. 1–3, Oct. 2019.

[6] S. Agostinelli *et al.*, "Geant4—a simulation toolkit," *Nuclear Instruments and Methods in Physics Research Section A: Accelerators, Spectrometers, Detectors and Associated Equipment*, vol. 506, pp. 250–303, July 2003.

[7] J. Allison *et al.*, "Geant4 developments and applications," *IEEE Transactions on Nuclear Science*, vol. 53, pp. 270–278, Feb. 2006.

[8] J. Allison *et al.*, "Recent developments in Geant4," *Nuclear Instruments and Methods in Physics Research Section A: Accelerators, Spectrometers, Detectors and Associated Equipment*, vol. 835, pp. 186–225, Nov. 2016.

[9] M. A. Green, "Self-consistent optical parameters of intrinsic silicon at 300K including temperature coefficients," *Solar Energy Materials and Solar Cells*, vol. 92, pp. 1305–1310, Nov. 2008.

[10] M. N. Polyanskiy, "Refractive index database." https://refractiveindex.info.

[11] "Hamamatsu S13615-1050N-16 Datasheet." hamamatsu.com/resources/pdf/ssd/s13615_series_kapd1062e.pdf.

[12] W. Falcon, "PyTorch lightning," *GitHub. Note: https://github.com/PyTorchLightning/pytorch-lightning*, vol. 3, 2019.

[13] L. Biewald, "Experiment tracking with weights and biases," 2020.

[14] K. He, X. Zhang, S. Ren, and J. Sun, "Deep Residual Learning for Image Recognition," *arXiv:1512.03385 [cs]*, Dec. 2015.

[15] D. P. Kingma and J. Ba, "Adam: A Method for Stochastic Optimization," *arXiv:1412.6980 [cs]*, Jan. 2017.